

Correlated Initialization for Correlated Data

Johannes Schneider¹

Abstract

Spatial data exhibits the property that nearby points are correlated. This holds also for learnt representations across layers, but not for commonly used weight initialization methods. Our theoretical analysis reveals for uncorrelated initialization that (i) flow through layers suffers from much more rapid decrease and (ii) training of individual parameters is subject to more “zig-zagging”. We propose multiple methods for correlated initialization. For CNNs, they yield accuracy gains of several per cent in the absence of regularization. Even for properly tuned L2-regularization gains are often possible.

1. Introduction

Highly non-linear models such as deep learning networks are commonly subject to iterative numerical optimization, which is often sensitive to initialization. Ideally, weights of a network are initialized at the global optimum rendering any form of optimization unnecessary. In the worst case, initialization is such that iterative optimization schemes are either not converging or inferior solutions are reached. Thus, an important question in deep learning is *How to initialize weights of a network?* This question has led to multiple works (Glorot & Bengio, 2010; Mishkin & Matas, 2015; Saxe et al., 2013; Zhang et al., 2019; Grosse et al., 2019). These papers commonly draw motivation by investigating behavior across layers to foster gradient flow based on aggregate properties of weights of a layer. In contrast, this paper investigates the behavior of weights of a single spatial filter, often consisting of 3×3 weights in modern convolutional neural networks (CNNs). CNNs encode the assumption that nearby points are most relevant to learn representations. This is justified largely by the observation that inputs are spatially correlated meaning that there are less dependencies between distant than between nearby points. Learnt representations often show strong differences between nearby points. For example, they might represent Gabor filters

^{*}Equal contribution ¹University of Liechtenstein, Liechtenstein. Correspondence to: Johannes Schneider <johannes.schneider@uni.li>.

(Coates et al., 2011) for edge detection. Still, overall correlation between adjacent filter weights is clearly positive as indicated in Figure 1. Correlation decreases with distance and increases with layers. Similar results were obtained for additional architectures such as VGG-16, InceptionV3, Xception, DenseNet121¹. We provide theoretical insights on convergence behavior showing that non-correlated initialization can drastically reduce gradient flow across layers and lead to more updates in opposing directions (“zig-zag”) for individual weights compared to correlated initialization. We also discuss common regularization schemes with respect to their impact on spatial correlation showing that L2-regularization fosters spatial correlation. The developed theory suggests that spatial weights of $k \times k$ filters should also initially be spatially correlated in the absence of L2-regularization. In the presence of L2-regularization gains might also be possible. We propose multiple methods for correlated initialization of CNNs that yield strong improvements on accuracy in the absence of L2-regularization. Often, they also improve networks with L2-regularization in place.

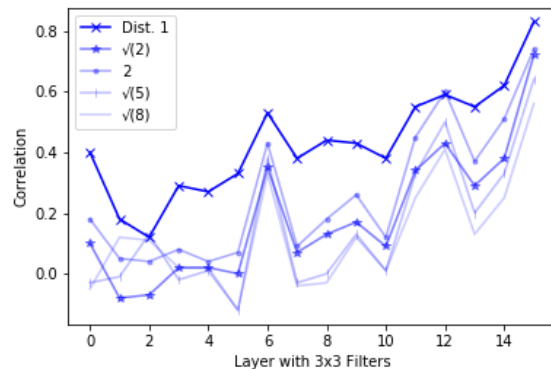


Figure 1. Distance-dependent correlation of weights of 3×3 filters ResNet50 trained on ImageNet

2. Within Layer, Single Filter Convergence

We discuss the interdependence of training data and gradient descent for a single $k \times k$ spatial filter w with ReLU activation and quadratic loss function, ie. $\hat{y} := \max(w \cdot X, 0)$ and $L(X, w) := (y - \hat{y})^2$. Weights w^* denote the optimal solution. We use $y(X) = w^* \cdot X$. This essentially expresses

¹all trained on ImageNet, available in the Keras framework

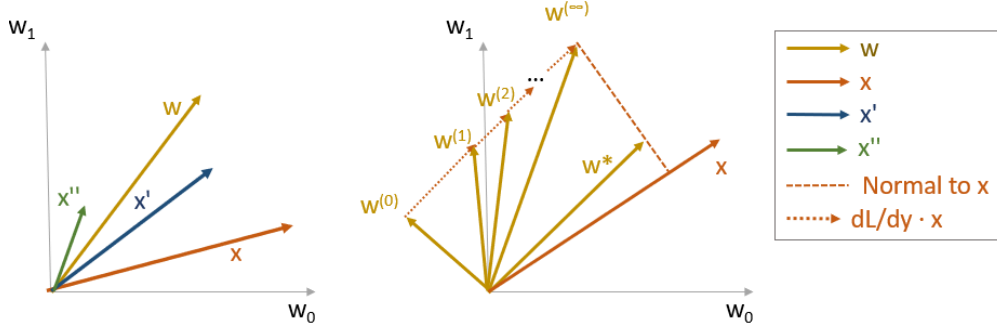


Figure 2. Left: Setup: 3 training samples X , X' and X'' and spatial filter $w = (w_0, w_1)$. Right: Training for one sample starting at $w^{(0)}$.

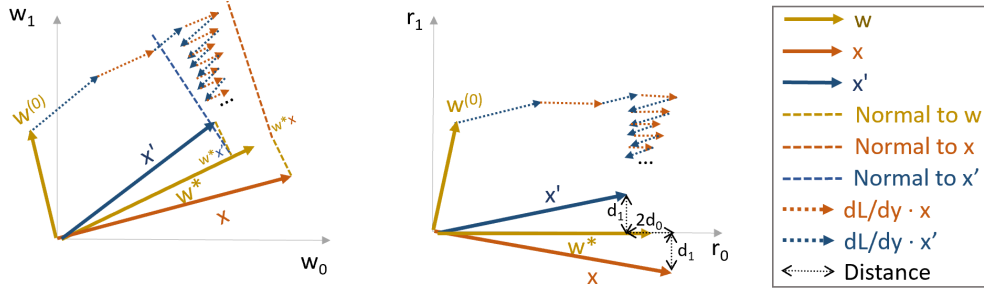


Figure 3. Training of two weights of a spatial filter for two training samples. Right: Rotated coordinate system with distances

the assumption that the spatial $k \times k$ filter followed by a ReLU is a suitable model. We discuss two scenarios: (i) The number of training samples is less than the number of parameters (under-determined system) and (ii) the number of training samples is at least as large as the number of parameters.

Under-determined system: Gradient descent can only explore the parameter space that is given by a linear combination of the base vectors (= span) of the training vectors with the initial vector added to it as a bias. The initialization expresses the prior belief of where a good solution is likely to be found. This belief also restricts the possible solutions that can be found. Thus, initialization has a profound impact on the quality of the solution. This can be seen by looking at the possible directions that a weight can be changed using gradient descent. The derivative of an aggregation layer $w \cdot x$ with respect to weight w_i is given by the input, ie. $dy/dw_i = x_i$. The derivative of the loss with respect to weight w_i is: $dL/dw_i = dL/dy \cdot dy/dw_i = dL/dy \cdot x_i$. Thus, dL/dy provides the magnitude of change and the inputs x_i provide the direction of the gradient vector ∇L_w . The weights w_i do not impact direction at all and the possible directions are entirely given by ∇L_w that depend only on the training samples.

The convergence behavior of an under-determined system is illustrated in the left panel of Figure 2 for a single training

example $(X, y) = (X, w^* X)$ and two weights.² Note that axis for weight dimensions w_j and inputs X_j overlap. Since there is only one training example the change of w can only be in the direction of the sample X . Thus, starting from an initial vector $w^{(0)}$ the vector w converges towards $w^{(\infty)}$ following a straight line. The final weights $w^{(\infty)}$ achieve zero training error, ie. $\hat{y} = w^{(\infty)} \cdot X = w^* \cdot X = y$. Still, they are dissimilar from the optimal weights w^* . Therefore, performance on unseen examples is negatively impacted.

(Over)-determined system: If the training samples span the entire parameter space then convergence of w to the optimal w^* is ensured for (adequate learning rates) due to the convex nature of the problem. However, the number of iterations to get close to the optimal solution is dependent on the initial conditions. This is indicated for two training samples in Figure 3. In the right panel, each coordinate w_j moves towards the optimal coordinate w_j^* in either a “zig-zag” or “straight” manner. Both coordinates start out moving straight. Once the weight vector w has crossed the normal towards X' , the zig-zagging begins. As shown in Figure 3, this indicates slow convergence. To keep it to a minimum, ideally, the initial vector $w^{(0)}$ and w^* point in the same direction and samples X and X' are at a large angle to w^* . Therefore, given that weights w^* are correlated, correlated initialization provides faster convergence.

²We might also assume a distorted $w^* X$, ie. $w^* X + \epsilon$, as discussed in more detail later.

Let us formalize and analyze the scenario in the right panel in Figure 3. For the optimal solution holds: $w^* = (w_0^*, 0)$. There is a set of two training samples $S = \{(X', y'), (X, y)\}$ that are symmetric around w^* with $X' = (1-d_0, d_1)$ and $X = (1+d_0, -d_1)$ for constants $d_0 \in [0, 1]$ and $d_1 \in [0, 1]$.³ Breaking symmetry, ie. moving w^* towards one of the two samples X or X' can widen or shrink the zig-zag zone between the normals to X and X' in Figure 3, but the qualitative behavior remains the same. We assume that X and X' have positive coordinates. This assumption is fulfilled for the (most) prevalent CNN architecture using batch-normalization followed by a ReLU unit. Small distances d_0 and d_1 imply strong correlation between inputs. For small distance d_1 , distance d_0 quantifies variation in strength of the input feature. For small d_0 , distance d_1 gives the variation in match of the input with the representation w^* . We (still) assume $y(X) = w^* X$. Adding noise or other terms $f(X)$ to the outputs, ie. assuming $y(X) = w^* X + f(X)$ can also widen or shrink the zig-zag zone between the normals to X and X' in Figure 3, but the qualitative behavior is identical.

We consider gradient descent on samples S for a fixed learning rate λ that is sufficiently small to ensure convergence:

$$w^{(i+1)} = w^{(i)} - \frac{1}{|S|} \sum_{X \in S} \lambda \nabla_w f(X, w) \quad (1)$$

$$\nabla_w f(X, w) = \begin{cases} -2((w^* - w) \cdot X) \cdot X, & \text{if } w \cdot X > 0 \\ 0, & \text{otherwise} \end{cases} \quad (2)$$

We derive the following equations under the assumption that all points are active, ie. a point X is active if $w \cdot X > 0$ for all samples X . Thus, it contributes to the direction of the gradient. We discuss a loosening of this assumption later.

Using $w^* = (w_0^*, 0)$ yields the following weight updates $\nabla_w f(X, w)$:

$$-\nabla_{w_j} f(X, w) = 2((w_0^* - w_0)X_0 - w_1 X_1)X_j \quad (3)$$

Next, we evaluate Equations (1) and (3) for $S = \{X, X'\}$ with samples $X = (1+d_0, -d_1)$ and $X' = (1-d_0, d_1)$. After a few algebraic modifications the following recurrences

³Adding symmetric points $(1+d_0, d_1), (1-d_0, -d_1)$ leads to essentially equal results. One might also assume that samples follow a 2d Gaussian distribution with d_0, d_1 as standard deviation for each dimension and w^* . But this comes at the price of more cluttered notation.

are obtained for each parameter w_j :

$$w_0^{(i+1)} = w_0^{(i)} + 2\lambda(d_0^2(w_0^* - w_0^{(i)}) - d_0 d_1 w_1^{(i)}) + 2\lambda(w_0^* - w_0^{(i)}) \quad (4)$$

$$w_1^{(i+1)} = w_1^{(i)} - 2\lambda(d_0 d_1 (w_0^* - w_0^{(i)}) + d_1^2 w_1^{(i)}) \quad (5)$$

The details of the derivation of Equations 4 and 5 are as follows for w_0 using $X = (1+d_0, -d_1)$ and $X' = (1-d_0, d_1)$ and Equation (3) first:

$$\begin{aligned} & -\nabla_{w_0} f(X, w) \\ &= \left(2((w_0^* - w_0)(1+d_0) - w_1(-d_1)) \right) \cdot (1+d_0) \\ &+ \left(2((w_0^* - w_0)(1-d_0) - w_1 d_1) \right) \cdot (1-d_0) \\ &= \left(2((w_0^* - w_0)(1+d_0) - w_1(-d_1)) \right) \\ &+ \left(2((w_0^* - w_0)(1-d_0) - w_1 d_1) \right) \\ &+ \left(2((w_0^* - w_0)(1+d_0) - w_1(-d_1)) \right) d_0 \\ &+ \left(2((w_0^* - w_0)(1-d_0) - w_1 d_1) \right) \cdot (-d_0) \\ &= 4((w_0^* - w_0) \\ &+ 2((w_0^* - w_0)d_0(1+d_0) - w_1(-d_1 d_0)) \\ &+ 2((w_0^* - w_0)(-d_0)(1-d_0) - w_1(d_1(-d_0))) \\ &= 4((w_0^* - w_0) \\ &+ 2((w_0^* - w_0)2d_0^2 + 2w_1(d_1 d_0)) \\ &= 4((w_0^* - w_0)(1+d_0^2) + w_1(d_1 d_0)) \end{aligned} \quad (6)$$

Analogously for w_1 :

$$\begin{aligned} & -\nabla_{w_1} f(X, w) \\ &= \left(2((w_0^* - w_0)(1+d_0) - w_1(-d_1)) \right) \cdot (-d_1) \\ &+ \left(2((w_0^* - w_0)(1-d_0) - w_1 d_1) \right) \cdot d_1 \\ &= 2((w_0^* - w_0)(-d_1)(1+d_0) - w_1(-d_1)^2) \\ &+ 2((w_0^* - w_0)d_1(1-d_0) - w_1 d_1^2) \\ &= 4(- (w_0^* - w_0)d_1 d_0 - w_1 d_1^2) \end{aligned} \quad (7)$$

Plugging Equations (6) and (7) into Equation (1) yields Equations 4 and 5. In the paper, there is a sign mistake for higher order terms, which however does not change any claims.

It becomes apparent that the magnitude of change of the two coordinates w_0 and w_1 can differ strongly. Equation (5)

implies that for small d_1 , w_1 moves slowly towards $w_1^* = 0$ (in the orthogonal direction of w^*), ie. the gap is reduced by less than $d_1 \cdot ((w_0^* - w_0^{(i)}) + w_1^{(i)})$. In contrast, even for small d_0 (and d_1) w_0 tends to move more quickly towards the optimal w_0^* . That is, the steps are of size $((w_0^* - w_0^{(i)}) + w_1^{(i)})$ not depending on d_0, d_1 (Equation (4)). This shows that it is highly preferable, if the initial vector points in the same direction as the optimal. A gap in length is not a major concern, since this gap can be fairly quickly reduced independent of the training data. Correlation of weights implies that weights are similar, which says that an optimal weight vector w^* is more likely to point in certain directions, ie. near a 45 degrees angle to all coordinate w_i^* . Therefore, if an optimal weight vector has similar weights then also initial weights should have similar weights, ie. weights should be correlated. Let us discuss initial conditions with respect to both positive and negative correlation. We restrict our discussion to the case, where $w_j^0 \in [0, 1]$. Negative w_1^0 is symmetric, ie. it behaves equivalently in a qualitative manner, as is evident from the above recurrences, ie. Equations (4) and (5). Setting $w_0^{(0)}$ to a negative value might violate the assumption that input samples are active, ie. $w \cdot X > 0$.⁴ If for all X holds $w \cdot X \leq 0$, there are no updates (known as ‘‘Dead ReLU’’) and w does not converge to w^* . The more samples X fulfill $w \cdot X \leq 0$ the slower convergence is. If the ratio of active to total samples is r , the magnitude of updates is lowered by a factor of r due to Equation (2). In the case of many initially inactive samples, convergence might become faster and then slower again. It becomes faster since samples eventually become active. It slows down when the zig-zagging starts.

3. Multi Layer Convergence

We show that expected outputs decrease exponentially faster for uncorrelated initialization than for (perfectly positively) correlated initialization and inputs. Thus, information cannot flow very well through many layers in the early phases of training for spatial weights initialized independently.

We consider an untrained network with l layers, where all weights have just been initialized. We perform a single (1d) convolution of weights w^i of width k in each layer i . The variables w_j^i are chosen either independently or such that they have positive correlation of 1. For correlated initialization, we set w_j^i to be identical to the first weight, which is randomly chosen: $w_j^i = w_0^i \forall j$. We choose a random weight w_0^i uniformly at random, ie. $w_0^i \sim U(-u, u)$. The limit u can be set using, for example, variance scaling (He et al., 2015). Inputs are perfectly correlated, ie. the elements of the input vector X^0 are set to a constant, ie. $X_j^0 = c^0 = 1$.

⁴Remember, by assumption (ReLU layer) all inputs X have non-negative coordinates.

Since the input X^0 to the first layer is constant, also the input X^i to any other layer is constant, ie. $X_j^i = c^i \forall j$. To avoid cluttered notation due to boundary conditions, we assume that for each layer the size of the input vector X^i is at least the size of the convolution, ie. k . We aim to estimate the magnitude of the expected output of the last layer, which is the same as the input to an additional layer $l + 1$, ie. $E[|c^l|]$.⁵

We compute the magnitude of inputs c^i for each layer i . We use $c^0 = 1$.

$$|c^{i+1}| = |w^i \cdot c^i| = |c^i| \left| \sum_{j < k} w_j^i \right| \quad (8)$$

$$|c^l| = |c^0| \cdot \prod_{i < l} \left| \sum_{j < k} w_j^i \right| = \prod_{i < l} \left| \sum_{j < k} w_j^i \right| \quad (9)$$

Next, we compute the expectation $E[|c^l|]$ using that weights are chosen independently across layers, ie. w_j^i and w_p^o are independent if $i \neq o$. This implies that $E[XY] = E[X]E[Y]$ and $E[|\sum_{j < k} w_j^i|] = E[|\sum_{j < k} w_j^o|] = E[|\sum_{j < k} w_j|]$:

$$\begin{aligned} E[|c^l|] &:= E\left[\prod_{i < l} \left| \sum_{j < k} w_j^i \right| \right] = \prod_{i < l} E\left[\left| \sum_{j < k} w_j^i \right| \right] \quad (10) \\ &= E[|S_k|]^l \text{ with } S_k := \sum_{j < k} w_j \end{aligned}$$

For correlated initialization, using Equation (10), $w_0 \sim U(-u, u)$ and linearity of expectation gives:

$$\begin{aligned} |w_0| &\sim U(0, u) \\ E[|S_k|] &= kE[|w_0|] = \frac{ku}{2} \\ E[|c^l|] &= \left(\frac{ku}{2}\right)^l = \left(\frac{1}{2} \cdot ku\right)^l \quad (11) \end{aligned}$$

For uncorrelated initialization we approximate S_k by the normal distribution using the central limit theorem.⁶

$$\begin{aligned} \overline{S}_k &= S_k/k \\ E[S_k] &= E[\overline{S}_k] = 0, \text{Var}[w_0] = u^2/12 \\ \frac{\sqrt{k}(\overline{S}_k - 0)}{u/\sqrt{12}} &= \sqrt{12k}/u \cdot \overline{S}_k = \sqrt{12k}/u \cdot S_k/k \rightarrow N(0, 1) \\ \text{Var}[\sqrt{12k}/u \cdot S_k/k] &= 1 \implies \text{Var}[S_k] = ku^2/12 \end{aligned}$$

Thus, $S_k \sim N(0, u^2k/12)$. Taking the magnitude of a normally distributed variable $Z \sim N(0, \sigma^2)$, yields a variable

⁵Using just the expected output $E[c^l]$ (without magnitude) yields 0, since $E[w_j^0] = 0$

⁶ S_k (with minor transformations) follows the Irwin-Hall distribution, which does not yield well-readable closed-form expressions.

following a half normal distribution $|Z| \sim HN(\sigma^2)$ with $E[|Z|] = \sigma \sqrt{2/\pi}$:

$$\begin{aligned} E[|S_k|] &= \sqrt{(ku^2)/12} \sqrt{2/\pi} = \sqrt{(ku^2)/(6\pi)} \\ E[|c^l|] &= E[|S_k|]^l = \left(\sqrt{\frac{1}{6\pi}} \cdot \sqrt{ku}\right)^l \approx \left(\frac{1}{4.3} \cdot \sqrt{ku}\right)^l \end{aligned} \quad (12)$$

Comparing the magnitude of the expected outputs for both initialization schemes (Equations 11 and 12), it becomes apparent that uncorrelated initialization leads to outputs that are less by a factor of about $(\sqrt{k}/2.3)^l = \Theta(k^{l/2})$. Therefore, also gradients for uncorrelated initialization are smaller.

4. Spatial Correlation and Regularization

L2-regularization and weight decay both make weights more equal by reducing weights w_i in each update by λw_i , where λ is a parameter denoting regularization strength. That is, large weights are reduced more in absolute terms. Thereby, they become more similar, ie. correlation increases among weights.

Batch-normalization(Ioffe & Szegedy, 2015) modifies entire input channels independently, impacting the scale and offsets of inputs to a spatial filter. This has no direct impact on spatial correlation of inputs. Therefore, we anticipate that correlated initialization is still beneficial given batch-normalization. Formally, this can be seen using the Pearson product moment coefficient for two random variables X, Y and substituting a transformation function $f(Z) = a_Z Z + b_Z$ as used in batch normalization:

$$\begin{aligned} E[f(Z)] &= a_Z \mu_Z + b_Z, & \sigma_{f(Z)} &= a_Z \sigma_Z \\ \rho_{X,Y} &:= \frac{E[(X - \mu_X)(Y - \mu_Y)]}{\sigma_X \sigma_Y} \\ &= \frac{E[(f(X) - \mu_{f(X)})(f(Y) - \mu_{f(Y)})]}{\sigma_{f(X)} \sigma_{f(Y)}} \end{aligned} \quad (13)$$

Similarly, **Dropout** (Srivastava et al., 2014) drops entire inputs, ie. all inputs of a spatial filter are set to zero. Dropping input features can be seen as noise reduction from the perspective of a single spatial filter. That is, the output of a feature aggregating all spatial filters is more strongly determined by the non-dropped filters. Therefore, also the updates during backpropagation are less impacted by other (irrelevant) spatial filters facilitating learning. This benefits weights that are initialized in a correlated or uncorrelated manner. Thus, we do not expect a strong interaction of dropout and initialization.

5. Correlated Initialization Methods

We propose correlated initialization for a single spatial $k \times k$ filter. We employ the idea that a spatial filter has a

“representation” center, where its strongest, with decreasing strength in surrounding locations implemented in Algorithm 1. The algorithm is illustrated in Figure 4. It chooses a location within the filter, sets its value randomly and assigns all other locations a discounted value depending on the distance. Then, it adds noise chosen independently to each location.

Algorithm 1 SingleFilterCorrInit

Input: Size k , nLayerWeights n_l , Locations L

Output: Initialization for $k \times k$ filter

- 1: $\alpha := 0.05$ {default; Fraction of random uncorrelated noise}
- 2: Decay function g :

$$g(d) := \begin{cases} 0 & a_0 := 1 \\ 1 & a_1 (= 0.9 \text{ default}) \\ \sqrt{2} & a_{\sqrt{2}} (= 0.7 \text{ default}) \\ 2 & a_2 (= 0.5 \text{ default}) \\ \text{otherwise} & a_{i>2} (= 0 \text{ default}) \end{cases}$$

- 3: $x_l, y_l :=$ Random location in L {“Representation center”}
 - 4: $s_m := 1/\sqrt{n_l}$ {Scaling similar to (He et al., 2015)}
 - 5: $s :=$ Random $[s_m, -s_m]$ {Strength at center x_l, y_l }
 - 6: $M_c := k \times k$ matrix initialized to 0
 - 7: **for** $x \in [0, k - 1]$ **do**
 - 8: **for** $y \in [0, k - 1]$ **do**
 - 9: $d := \sqrt{(x_l - x)^2 + (y_l - y)^2}$
 - 10: $M_c(x, y) := s \cdot g(d)$
 - 11: $M_r := k \times k$ matrix with entries chosen uniformly, independently at random in $[-s_m, s_m]$
 - 12: **return** $(1 - \alpha) \cdot M_c + \alpha \cdot M_r$
-

In more detail, for each spatial $k \times k$ filter, the algorithm picks randomly a location l of a pre-defined set of locations L . The location serves as the “representation” center. That is, the filter is most sensitive at this location, since the corresponding weight has largest magnitude. We employ the following sets of locations L :

- 1) ‘**all**’ locations: All $k \times k$ locations, $L := \{l | l \in [0, k - 1] \times [0, k - 1]\}$
- 2) ‘**cen**(ter)’ location: Using only the center $L := \{(1, 1)\}$
- 3) ‘**nei**(ghbor)’ locations: Locations at distance 1 from center, $L := \{(1, 0), (1, 2), (0, 1), (2, 1)\}$

The same set of locations L is used across all spatial filters for all layers. For the chosen location $l \in L$, the algorithm picks a strength s uniformly at random. It assigns all other locations at distance d a discounted value $s \cdot g(d) \leq s$. Distance is measured using indexes. As decay function g , expressing the degree of correlation with the representation center, functions like a Gaussian seem adequate. However,

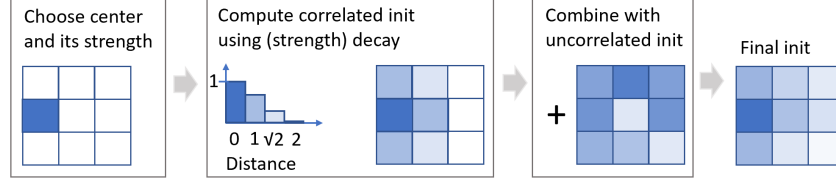


Figure 4. Illustration of Algorithm 1 for correlated initialization

we found better results when defining g with a fixed set of values. That is, for each distance $d \in \{0, 1, \sqrt{2}, 2, \sqrt{5}, \sqrt{8}\}$ we defined $g(d) := a_d$ with a_d being some fixed value and $a_0 := 1$. The algorithm computes a second uncorrelated initialization (matrix). Then, it calculates the weighted mean of both initialization matrices using weights $1 - \alpha$ for the correlated matrix and α for the uncorrelated matrix. Small α gave best results, eg. $\alpha \in [0, 0.2]$. For both matrices we employ scaling analogous to (He et al., 2015).⁷ Note that our initialization impacts variance, which requires adaption to be aligned with the ideas in (He et al., 2015) though given the use of batch-normalization this might not be needed in practice. The adaption depends on details of the initialization scheme, ie. locations L , distance decrements $g(i)$ and α . As example, we derive scaling factors for the center strategy for 3×3 filters for $\alpha = 0$. Using Algorithm 1 with $L = [(1, 1)]$ and general distance function g yields the following for the correlated weight matrix $M_c = w = (w_{i,j})$:

$$w_{i,j} = w_{1,1} \cdot g(d(i,j)) \quad (14)$$

$$\text{with } d(i,j) := \sqrt{(i-1)^2 + (j-1)^2} \quad (15)$$

This implies for bounding $\text{Var}(w)$ using $\text{Cov}(X, aX) = a\text{Var}(X)$:

$$\text{Var}(w) = \sum_{i,j,l,m < k} \text{Cov}(w_{i,j}, w_{l,m}) \quad (16)$$

$$\begin{aligned} \text{Cov}(w_{i,j}, w_{k,l}) &= \text{Cov}(w_{1,1} \cdot g(d(i,j)), w_{1,1} \cdot g(d(k,l))) \\ &= g(d(i,j)) \cdot g(d(k,l)) \cdot \text{Cov}(w_{1,1}, w_{1,1}) \end{aligned}$$

$$\begin{aligned} \text{Var}(w) &= (1 + 8g(1) + 8g(\sqrt{2}) + 16g(1)^2 \\ &+ 32g(1)g(\sqrt{2}) + 16g(\sqrt{2})^2) \end{aligned} \quad (17)$$

Assuming we have n_l/k^2 spatial filters and we want $\text{Var}(W) = 1$ for the entire layer W , we get as scaling constant s_m with $\text{Var}(w)$ defined in Equation 17:

$$s_m = \sqrt{\frac{k^2}{n_l \text{Var}(w)}} = \frac{k}{\sqrt{n_l \text{Var}(w)}} \quad (18)$$

⁷We scaled weights of a layer with n_l weights using $\sqrt{1/n_l}$, instead of $\sqrt{3/n_l}$ for uniform distribution (He et al., 2015). We found that this makes no difference for uncorrelated and correlated initialization, which is not surprising given the use of batch-normalization and networks of limited depth.

6. Experiments and Evaluation

Our experiments assess the following:

- Which proposed correlated initialization method is best? We compare three correlated initialization methods for different parameter settings and two network architectures (Sections 6.2 and 6.3).
- How is the interaction with different regularization methods? Claims in Section 4 show that regularization also impacts spatial correlation (Section 6.4) and, thus, likely it also influences the impact of correlated initialization.
- How is the interaction with model size – both depth and width? (Section 6.5).
- How is the performance if hyper-parameters are tuned and training data are augmented? (Section 6.6)
- How is the impact of dataset size? (Section 6.7)
- How is the impact of spatial filter size? Does correlated init enable larger filter sizes? (Section 6.8)
- How is the convergence speed w/o batchnorm layer? Based on theory (Sections 2 and 3) one would expect faster convergence (at least) initially without batchnorm (Section 6.9).
- How is the convergence and generalization performance based on the maximum, ie. initial, learning rate? One might suppose that correlated init benefits less from high learning rates, since the solution is supposedly closer to a good solution, ie. in the “error landscape” it must cross less valleys and gaps to reach a good solution (Section 6.10).

6.1. Setup and Analysis

We used a default setup, that was varied in one or more parameters for individual experiments. SGD with momentum 0.9 with batchsize 256 served for training. 39 epochs were sufficient to achieve a training error of mostly below 1×10^{-5} . We decayed the initial learning rate of 0.12 by 0.3 at epochs 19, 27, 33, and 37. Weights of dense layers were L2-regularized with 0.0005, other weights were not

regularized. We employed CIFAR-10/100(Krizhevsky & Hinton, 2009) without data augmentation and pre-defined split into training and test data.⁸ As networks, we used a VGG-10 variant and Resnet-10 (Table 1). For uncorrelated initialization we used uniform initialization (He et al., 2015) and for correlated initialization the defaults as in Algorithm 1 with nei(ghbor) initialization (See Strategy 3) in Section 5). We trained 10 networks for each configuration, ie. hyperparameter setting. We report average accuracy and standard deviation (indicated as shaded area in plots).

ResNet-10 (He et al., 2016)			VGG-10 variant (Simonyan & Zisserman, 2014)	
Block	Type/Stride	Filter Shape	Type/Stride	Filter Shape
-	C/s1	3×3×3×16	C/s1	3×3×3×16
1	C/s2	3×3×16×16	C/s2	3×3×16×16
	C/s1	3×3×16×32	C/s1	3×3×16×32
2	C/s2	3×3×32×32	C/s2	3×3×32×32
	C/s1	3×3×32×64	C/s1	3×3×32×64
3	C/s2	3×3×32×64	C/s2	3×3×64×64
	C/s1	3×3×64×64	C/s1	3×3×64×128
4	C/s2	3×3×64×128	C/s2	3×3×128×128
	C/s1	3×3×128×128	C/s1	3×3×128×256
5	C/s2	3×3×128×256	C/s2	3×3×256×256
	C/s1	3×3×256×256		
-	FC/s1	256×nClasses	FC/s1	256×nClasses
-	SoftMax/s1	Classifier	SoftMax/s1	Classifier

Table 1. Base Architectures. “C” is a convolutional layer and “FC” a dense layer; For ResNet we add to the output B of each block, the output of a $C/s1$ layer of shape $1 \times 1 \times B_d^i \times B_d^o$ (with B_d^i/B_d^o being the in-/output feature channels of the block); A BatchNorm and ReLU layer followed each “C” layer.

6.2. Correlated Initialization Methods

Figure 5 shows the outcomes for the three correlated initialization methods proposed in Section 5 with various spatial decay parameters a_i . Extending correlation to distance beyond one of the representation center yields some improvements. But using non-zero correlation for weights at distance 2 or larger has little impact. All initialization methods perform best for fairly large parameters a_i . The “cen”(ter) method seems best for ResNet, whereas the “nei”(ghbor) and “all” methods perform better for VGG. But this is partially due to the fact that there is too little noise for “cen”, ie. α is too large as assessed in Section 6.3. The gains using correlated initialization are more profound for VGG than ResNet, which is expected since the residual connections propagate correlated inputs through the network. Another explanation is that correlated initialization helps with larger gradient flow, but for ResNet gradient flow is less of a concern reducing the impact of this advantage.

6.3. Fraction of Uncorrelated Initialization

We also altered the amount of (uncorrelated) random noise as given by $1 - \alpha$ in Algorithm 1. Figure 6 highlights that

⁸see supplementary material for more datasets

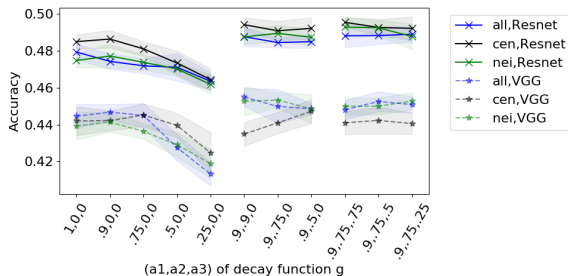


Figure 5. Accuracy on CIFAR-100 for corr. init. methods

the fraction of uncorrelated noise $1 - \alpha$ should be below 20% for all methods. Even without any uncorrelated noise, only the “center” method degenerates significantly. Generally, the more randomness a method introduces on its own, the less additional noise is needed, ie. the “center” method yields identical initialization for all spatial filters up to a constant factor. The “neighbor” method adds more noise due to random choice of one out of 4 locations for each spatial filter. The “all” method tops this by choosing one out of 9 locations. While outcomes of methods differ for the same parameter settings (a_i and α), there are no strong differences between methods if parameters a_i and α are tuned for each method.

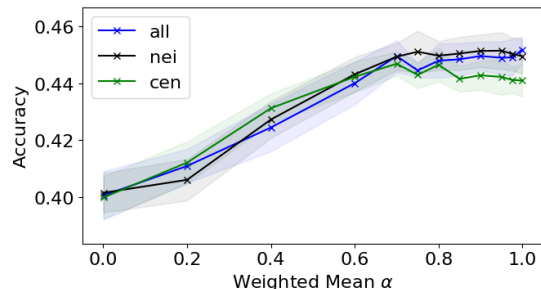


Figure 6. Accuracy on CIFAR-100 for varying α

6.4. Regularization

We investigated the interaction of correlated initialization and L2 regularization(Figure 7), DropOut(Figure 8) and batch-normalization. For batch-normalization (BN), we removed all BN layers and prolonged training by a factor of 2. Correlated and uncorrelated initialization show a gap of about 5% w/o BN, ie. accuracy on CIFAR-100 for correlated init w/o BN is 0.445 / 0.241 and for uncorrelated init w/o BN it is 0.395 / 0.192. Based on the theoretical analysis (Section 4), a similar gap is indeed expected. Correlated and uncorrelated initialization both benefit from L2 and dropout regularization. For L2-regularization networks with uncorrelated initialization exhibit much larger gains (as expected based on theory). For ResNet L2-regularization gains due to correlated initialization are more diminished

than for VGG (see Section 6.2 for a reasoning). For dropout, we added a dropout layer after layers 4, 8 and 10. The gains are somewhat larger for uncorrelated initialization, but a large gap remains between both initialization schemes.

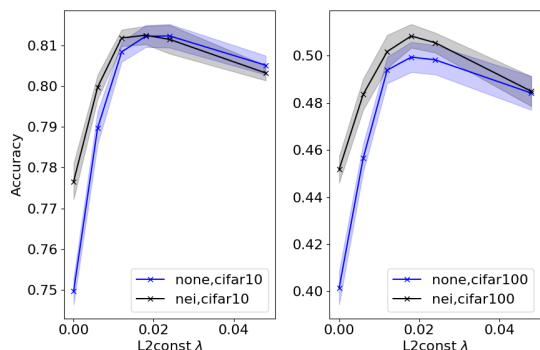


Figure 7. Accuracy on CIFAR-10(left) and CIFAR-100(right) using L2 regularization

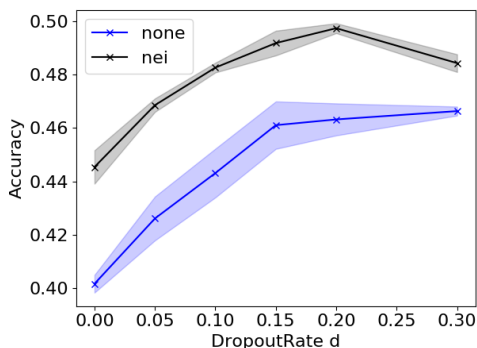


Figure 8. Accuracy on CIFAR-100 for varying DropOut rates

6.5. Width and Depth

We investigate modifications of Resnet using 60 epochs of training (with decay epochs also scaled by a factor of 1.5). Figure 9 shows that the gap between the two initialization schemes seems to grow up to some point, when increasing either depth or width.

6.6. Data augmentation and L2-Regularization

We used heavy data augmentation (translation, rotation, horizontal flipping and cropping). We also used the FASHION-MNIST(Xiao et al., 2017) and ‘Rock-paper-scissors’ dataset.⁹ Training and decay epochs(Section 6.1)

⁹available through Tensorflow; Dataset URL: <http://laurencemoroney.com/rock-paper-scissors-dataset>. It consists of 2520 training and 372 text images of 300x300 pixels with 3 channels that we scaled to size 128x128. Since the dataset is fairly simple consisting of only 3 classes, we used our ResNet architecture with a total of 7 blocks and just 2x16,2x32,2x64,1x128 output neurons

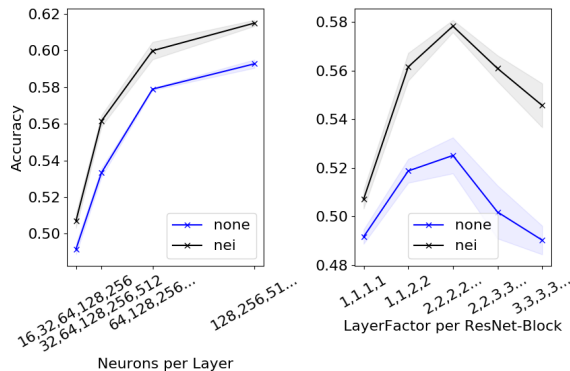


Figure 9. Accuracy on CIFAR-100 for depth and width of ResNet

were increased by a factor of 6 and batchsize was 128. We use a Resnet-18, ie. each of the four blocks in Table 1 got duplicated in depth and the number of neurons of each layer was increased by a factor of two. We used L2 regularization with parameter λ with values from 1×10^{-4} to 2.56×10^{-2} in steps incremented by a factor 1.5.¹⁰ The average and standard deviation of five.¹¹ runs for the best λ are shown in Table 2. A t-test on means for correlated and uncorr. init yielded p-values above 0.2.

Init	CIFAR-100	CIFAR-10	FASHION-M.	Rock-P-S.
Uncorr.	.74 ± .021	.942 ± .007	.944 ± .008	.917 ± .031
Corr.	.74 ± .019	.947 ± .004	.948 ± .003	.917 ± .027

Table 2. Accuracy with data augmentation for L2-reg.

Additionally, we trained on the ‘Tiny-ImageNet’ dataset¹² consisting of 200 classes, 100000 training and 10000 test samples of size 64x64x3. We adjusted our VGG-10 architecture by adding 3 more conv layers with output neurons increasing from 64 to 1024. We added also two dropout layers, one in the middle and one before the dense layer with dropout rates 0.1 and 0.15. There, we also did not find statistically significant differences in accuracy, ie. with uncorrelated initialization we achieved $55.4\% \pm 0.3\%$ and with correlated init $55.39\% \pm 0.25\%$. This shows that while there might be significant differences for larger models or less training data, they seem to be only modest under L2-regularization tuning and heavy data augmentation.

6.7. Amount of data

Figure 10 shows the behavior when increasing the amount of training data and using 80 epochs. Interestingly, there is of blocks (Larger networks gave worse accuracy).

¹⁰It was two.

¹¹It was three.

¹²<https://tiny-imagenet.herokuapp.com/>

a sweet-spot, where gains are largest. For data quantities tending to infinity, correlated and uncorrelated init seems to converge to the same accuracy. For the CIFAR-10 dataset, however, the type of spatial initialization still matters, but to a lesser extent.

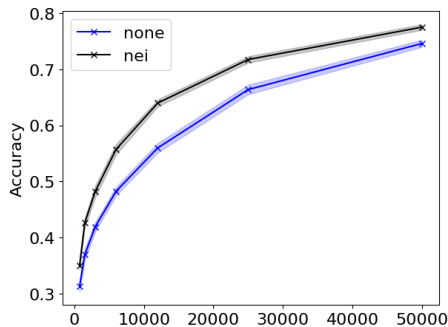


Figure 10. Accuracy on CIFAR-10 depending on the dataset size

6.8. Larger Spatial Filters

Figure 11 shows the behavior for filter sizes 3×3 , 5×5 and 7×7 when trained with the number of epochs scaled by a factor of 2 (also for decay) for our VGG variant.¹³

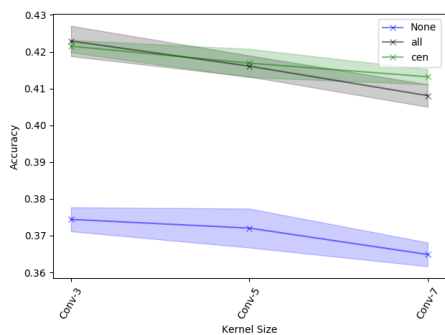


Figure 11. Accuracy on CIFAR-100 depending on filter size

6.9. Convergence Speed

Figures 12 and 13 show the convergence behavior for our VGG network without batchnorm(BN) layers when multiplying training and decay epochs by a factor of 6. Aligned with theory correlated initialization leads to faster convergence in the first epochs of training (see Figure 12) manifesting in higher training and validation accuracy. While validation accuracy stays higher for correlated initialization, interestingly, training accuracy for non-correlated init catches up at about epoch 20. It seems also less stable, ie. it

starts to oscillate shortly before the first decay of the learning rate (Figure 13). We also considered VGG with BN layers where we trained for 60 epochs (Figure 14). Learning is much faster for both methods. There is no more initial advantage in convergence speed for correlated initialization, when measuring after each epoch.

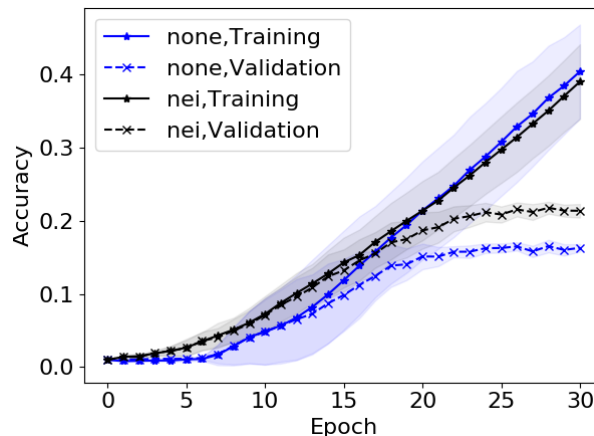


Figure 12. Accuracy on CIFAR-100 for VGG-10 without BN for epochs ≤ 30

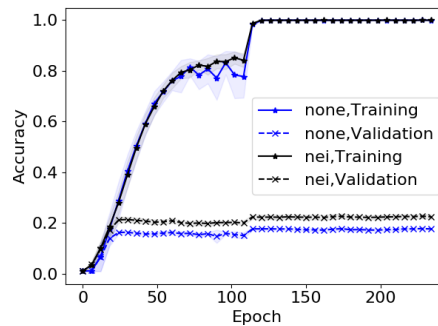


Figure 13. Accuracy on CIFAR-100 for VGG-10 without BN

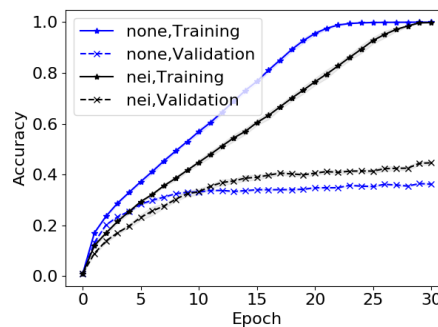


Figure 14. Accuracy on CIFAR-100 for VGG-10 with BN

¹³The neurons in the last layer were only 128 instead of 256.

6.10. Initial Learning Rate and Generalization

Figure 15 shows final accuracy based on the initial learning rate, where training was stretched by a factor of two to ensure that a training error of close to zero was reached even for low initial learning rates. Both benefit from larger initial learning rates. But the sensitivity is much larger for non-correlated initialization. That is, uncorrelated init benefits more from larger learning rate. This is expected based on our theoretical investigation. Intuitively, correlated initialization is closer to optimized weights, which are also correlated (Section 1). Therefore, weight vectors must move less far on the loss landscape to reach good solutions, which decreases the risk that weight vectors cannot escape not so good local optima for low learning rates. For the sake of completeness, we also altered the decay factor, ie. we tried 0.1, 0.2, 0.4, 0.8. However, neither method improved or worsened more than 0.3%, except non-correlated initialization for 0.8 indicating that the learning rate is not decreased sufficiently overall.

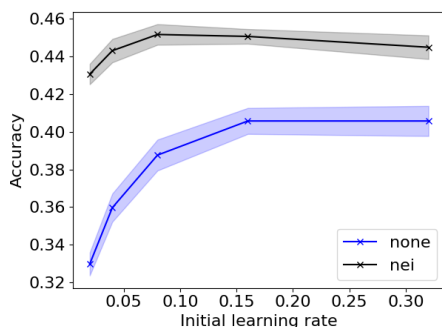


Figure 15. Accuracy on CIFAR-100 depending on initial learning rates

7. Related Work

Initialization schemes have often been designed to allow training of very deep networks. (Glorot & Bengio, 2010) monitored activations and gradients and utilized the idea that variance of layer (inputs) should stay the same across layers to encourage flow of information through the network. The derivation in (Glorot & Bengio, 2010) does not account for non-linearities. Altering the derivation including rectified linear units (ReLU) led to the “He” initialization (He et al., 2015). “He” initialization seems also to be favorably related to over-parameterization of networks (Arpit & Bengio, 2019). Similar to these early works, more recent work has also considered activation scale (Hanin & Rolnick, 2018) and gradients (Balduzzi et al., 2017) as well as dynamical isometry properties (Saxe et al., 2013; Yang & Schoenholz, 2017). In contrast, we are not primarily concerned with depth, eg. the vanishing and exploding gradient problem, but focus on deriving initialization for a single spatial filter.

Initializing networks by training on another dataset is common in transfer learning. It has been said to yield better performance and faster training. Recent work (He et al., 2019) has challenged this wisdom by providing examples where random initialization leads to as good performance compared to pre-training and fine-tuning, albeit at a potential longer training time. Still, using some form of data-dependent initialization can improve convergence speed (Aguirre & Fuentes, 2019; He et al., 2019).

Normalization and Initialization: There is also a relationship between batch normalization (Ioffe & Szegedy, 2015) and weight initialization. (Mishkin & Matas, 2015) extends an orthonormal initialization (Saxe et al., 2013) with unit-variance. They perform batch normalization only on the very first mini-batch given orthonormal initialization. This allows them to avoid the computational costs of batch-normalization but they do not claim any accuracy gains compared to relying on batch-normalization only. (Zhang et al., 2019) shows that using proper initialization instead of normalization (layers) for residual networks yields equal performance. The focus is primarily on avoiding issues in training due to exploding or vanishing gradients. Theoretical underpinnings for batch normalization are still subject to discussion. Its success has been attributed to internal covariate shift (Ioffe & Szegedy, 2015) and smoother loss surface (Santurkar et al., 2018). (Luo et al., 2018) claims that regularization in the context of batch-normalization is accomplished due to noise injection on inputs.

Other: Other work has also considered spatial properties, ie. (Schneider, 2019) derived a regularization scheme arguing that central weights in a spatial filter should be regularized less. They argue that in this case representations exhibit desirable properties such as larger cohesion. It is rooted on empirical findings that central weights of spatial filter are larger. Later, this observation has also been leveraged through architectural changes (Ding et al., 2019). (Kuo, 2016) analyzed also convolutional layers in combination with a ReLU, discussing why ReLUs are needed. They view ReLUs as eliminating inputs that are negatively correlated with the representation. We also discuss “Dead” ReLUs from the perspective of spatial correlation, whereas other work (Lu et al., 2019) analyzed this phenomena without taking spatial correlation into account claiming that depth impacts gradient flow negatively.

8. Conclusions

This work used theoretical and empirical analysis to deepen the understanding of networks leveraging correlated input data. Correlated init. fosters gradient flow and reduces “zig-

zagging” during training. It can lead to better generalization.

References

- Aguirre, D. and Fuentes, O. Improving weight initialization of relu and output layers. In *International Conference on Artificial Neural Networks*, pp. 170–184, 2019.
- Arpit, D. and Bengio, Y. The benefits of over-parameterization at initialization in deep relu networks. *arXiv preprint arXiv:1901.03611*, 2019.
- Balduzzi, D., Frean, M., Leary, L., Lewis, J., Ma, K. W.-D., and McWilliams, B. The shattered gradients problem: If resnets are the answer, then what is the question? In *Proc. of the International Conference on Machine Learning (ICML)*, pp. 342–350, 2017.
- Coates, A., Ng, A., and Lee, H. An analysis of single-layer networks in unsupervised feature learning. In *International conference on artificial intelligence and statistics (AISTats)*, pp. 215–223, 2011.
- Ding, X., Guo, Y., Ding, G., and Han, J. Acnet: Strengthening the kernel skeletons for powerful cnn via asymmetric convolution blocks. In *Proc. of the International Conference on Computer Vision*, pp. 1911–1920, 2019.
- Glorot, X. and Bengio, Y. Understanding the difficulty of training deep feedforward neural networks. In *Proc. of the international conference on artificial intelligence and statistics*, pp. 249–256, 2010.
- Grosse, K., Trost, T. A., Mosbach, M., Backes, M., and Klakow, D. Adversarial initialization—when your network performs the way i want. *arXiv preprint arXiv:1902.03020*, 2019.
- Hanin, B. and Rolnick, D. How to start training: The effect of initialization and architecture. In *Advances in Neural Information Processing Systems*, pp. 571–581, 2018.
- He, K., Zhang, X., Ren, S., and Sun, J. Delving deep into rectifiers: Surpassing human-level performance on imagenet classification. In *Proc. of the international conference on computer vision*, pp. 1026–1034, 2015.
- He, K., Zhang, X., Ren, S., and Sun, J. Deep residual learning for image recognition. In *Proc. of the conference on computer vision and pattern recognition*, pp. 770–778, 2016.
- He, K., Girshick, R., and Dollár, P. Rethinking imagenet pre-training. In *Proc. of the International Conference on Computer Vision*, pp. 4918–4927, 2019.
- Ioffe, S. and Szegedy, C. Batch normalization: Accelerating deep network training by reducing internal covariate shift. *arXiv preprint arXiv:1502.03167*, 2015.
- Krizhevsky, A. and Hinton, G. Learning multiple layers of features from tiny images. Technical report, 2009.
- Kuo, C.-C. J. Understanding convolutional neural networks with a mathematical model. *Journal of Visual Communication and Image Representation*, 41:406–413, 2016.
- Lu, L., Shin, Y., Su, Y., and Karniadakis, G. E. Dying relu and initialization: Theory and numerical examples. *arXiv preprint arXiv:1903.06733*, 2019.
- Luo, P., Wang, X., Shao, W., and Peng, Z. Towards understanding regularization in batch normalization. *arXiv preprint arXiv:1809.00846*, 2018.
- Mishkin, D. and Matas, J. All you need is a good init. *arXiv preprint arXiv:1511.06422*, 2015.
- Santurkar, S., Tsipras, D., Ilyas, A., and Madry, A. How does batch normalization help optimization? In *Advances in Neural Information Processing Systems*, pp. 2483–2493, 2018.
- Saxe, A. M., McClelland, J. L., and Ganguli, S. Exact solutions to the nonlinear dynamics of learning in deep linear neural networks. *arXiv preprint arXiv:1312.6120*, 2013.
- Schneider, J. Locality-promoting representation learning. *arXiv preprint arXiv:1905.10661*, 2019.
- Simonyan, K. and Zisserman, A. Very deep convolutional networks for large-scale image recognition. *Int. Conference on Learning Representations (ICLR)*, 2014.
- Srivastava, N., Hinton, G., Krizhevsky, A., Sutskever, I., and Salakhutdinov, R. Dropout: a simple way to prevent neural networks from overfitting. *The journal of machine learning research*, 15(1):1929–1958, 2014.
- Xiao, H., Rasul, K., and Vollgraf, R. Fashion-mnist: a novel image dataset for benchmarking machine learning algorithms. *arXiv preprint arXiv:1708.07747*, 2017.
- Yang, G. and Schoenholz, S. Mean field residual networks: On the edge of chaos. In *Advances in neural information processing systems*, pp. 7103–7114, 2017.
- Zhang, H., Dauphin, Y. N., and Ma, T. Fixup initialization: Residual learning without normalization. *arXiv preprint arXiv:1901.09321*, 2019.